

How Are Non-Bonded G···Z (Z = O, S, and Se) Distances at Benzene 1,2-, Naphthalene 1,8-, and Anthracene 1,8,9-Positions Controlled? An Approach to Causality in Weak Interactions

Satoko Hayashi and Waro Nakanishi*

Department of Material Science and Chemistry, Faculty of Systems Engineering, Wakayama University, 930 Sakaedani, Wakayama 640-8510

Received October 22, 2008; E-mail: nakanisi@sys.wakayama-u.ac.jp

Mechanisms operating in weak interactions are sometimes quite different from those in strong ones. Factors to control the non-bonded G···Z (Z = O, S, and Se) distances at naphthalene 1,8-positions in 8-G-1-RZ$C_{10}H_6$ are analyzed as an example to clarify the causality of weak interactions. Structures around Z in 8-G-1-RZ$C_{10}H_6$ are well explained by three types, **A**, **B**, and **C**, where the Z–C_R bond is perpendicular to the naphthyl plane in **A**, it is placed on the plane in **B**, and **C** is intermediate between **A** and **B**. The r(Z···Z) distances in 1,8-$(RZ)_2C_{10}H_6$ are observed to increase in an order of **BB** < **CC** < **AB** < **AA**. It seems difficult to explain the sequence based on the magnitudes of the closed-shell Z···Z interactions, since the **BB** interaction must not be so strong especially for Z of heavier atoms. The mechanism to control the r(Z···Z) distances is demonstrated to be the reflection from the repulsive interactions between R and H at the 2-position in 1,8-$(RZ)_2C_{10}H_6$. Similar phenomena are also detected in the observed and calculated results at the benzene 1,2-, anthracene 1,8,9-, and anthraquinone 1,8,9-positions, which are explained based on the mechanism. Proposed idea and mechanism will help us to understand what happens in such weak interactions.

Weak interactions as factors to control fine structures are of current interest.[1–3] While strong interactions or strong bonds set up the framework of molecules, weak interactions control fine structures of molecules or create high functionalities of materials. We are highly interested in weak interactions of the closed-shell type[4] between group 16 elements.[5] Atomic orbitals at non-bonded atoms in each molecule or parts of a molecule will directly overlap, when the atoms come closer than the sum of the van der Waals radii (r_{vdW}). The direct orbital overlaps at distances less than the sum of r_{vdW} will be attractive, if the exchange repulsion[6] is suitably controlled.[5,7] An effort has been made to elucidate the factors to control the fine structures of 1,8-disubstituted naphthalenes, anthracenes, and/or anthraquinones based on weak interactions:[8] It is also clarified how weak interactions operate to determine the fine structures. However, it is still often difficult to demonstrate the causality in phenomena arising from weak interactions, with physical necessity. Each phenomenon in question should be analyzed as the result of the weak interaction, if it is the real cause. One could mistake superficial for the real causes, since weak interactions usually operate behind other factors of superficial contributions. There could also exist such cases that phenomena can be well explained at first glance by a weak interaction, but it is not the real cause.

Observed phenomena in substantially strong interactions are well explained by a simple syllogism. Scheme 1 explains the mechanism. Let result-**R1** be strongly coupled with cause-**S1**. Result-**R1** will give rise to another phenomenon, result-**R2**: result-**R1** becomes cause-**S2** in this process. Namely, cause-**S2**, derived from result-**R1**, gives rise to the next phenomena, result-**R2**. Result-**R2** will also be well explained by cause-**S2**, since result-**R2** is strongly coupled with cause-**S2**, compared with others. It is easily accepted, if the observed results in weak interactions are explained similarly to the case of the strong interactions.[2,3,9,10] However, the causality in weak interactions is sometimes quite different from those explained in the strong interactions, since weak interactions usually operate behind other factors of superficial contributions. We shed light on a typical case of the causality in weak interactions that originate from the G···Z interactions of the closed-shell type.

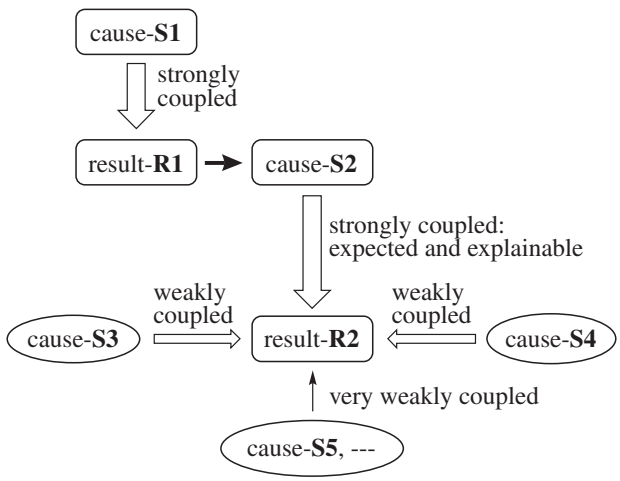

Scheme 1. Causality in strong interactions.

Published on the web June 12, 2009; doi:10.1246/bcsj.82.712

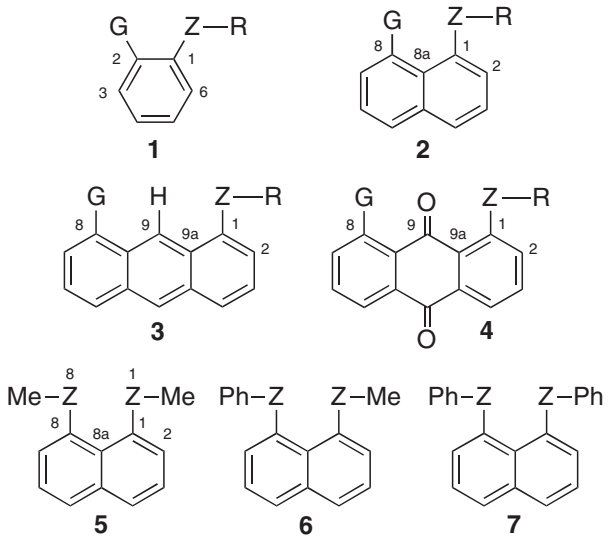

Chart 1. Compounds **1**–**7**.

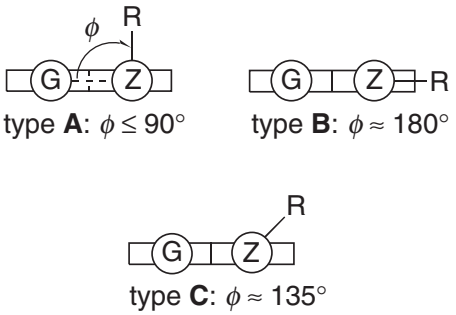

Scheme 2. The **A**, **B**, and **C** structures exemplified by 8-G-1-$RZC_{10}H_6$ (**2**).

Benzene 1,2-, naphthalene 1,8-, and anthracene 1,8,9-positions provide a good system to study weak interactions.[5,11,12] Anthraquinone 1,8,9-positions are also important to investigate such interactions. 2-G-1-RZC_6H_4 (**1**), 8-G-1-$RZC_{10}H_6$ (**2**),[5f,11b] 8-G-1-$RZC_{14}H_8$ (**3**),[13] and 8-G-1-$RZC_{14}H_6O_2$ (**4**)[13,14] are basic structures of our investigations, where Z = O, S, and Se, G = H, ZR′, and halogens with R and R′ = Me and Ar (Chart 1). Various types of closed-shell G···Z interactions are observed for non-H G. Tellurium-containing compounds are also contained in Chart 1, since the conclusions obtained based on the oxygen-, sulfur-, and selenium-containing compounds could also be applied to the tellurium-containing compounds. And Table 2 contains some data for **2** (ZR, G) = (TeR, TeR′).

Structures around Z in 8-G-1-$RZC_{10}H_6$ are well explained by three types, **A**, **B**, and **C**. Scheme 2 shows the **A**, **B**, and **C** conformers. The Z–C_R bond is perpendicular to the naphthyl plane in **A**, it is placed on the plane in **B**, and **C** is intermediate between **A** and **B**.[5b,5d–5f,5h,12b]

Various structures and interactions are observed in bischalcogenides, 1,8-$(MeZ)_2C_{10}H_6$ (**5**),[15–17] 8-PhZ-1-$MeZC_{10}H_6$ (**6**),[5a,5c,5e,17] and 1,8-$(PhZ)_2C_{10}H_6$ (**7**),[17–19] where **5**–**7** correspond to **2** (G = ZMe, ZR = ZMe), **2** (ZPh, ZMe), and **2** (ZPh, ZPh), respectively. Closed-shell Z···Z interactions have been widely investigated and discussed in relation to the factors to control the fine structures of **5**–**7**.[3,5f,5i,6,7,20] σ-Type three center–four electron interactions [σ(3c–4e)], σ(2c–4e), π(2c–4e), and distorted π(2c–4e) are the typical cases, which play an important role to determine the fine structures. The combined notation, **AA**-*t* (**A**-conformers around two Z–C_{Ar} bonds with R and R′ being trans configuration with each other), **AB**, **BB**, and **CC**,[5c,5g,17,20] is applied. Scheme 3 shows the combined notation for **1**–**4** where G in **1**–**4** are ZR′, X = H and OMe in **3**, and X = O in **4**. The typical structures of **5**–**7** are well expressed by the combined notation. Factors to control fine structures of **5**–**7** are of high interest.[17] However, we point out that factors to control the Z···Z distances, *r*(Z···Z), are also very important to understand the causality in weak interactions.

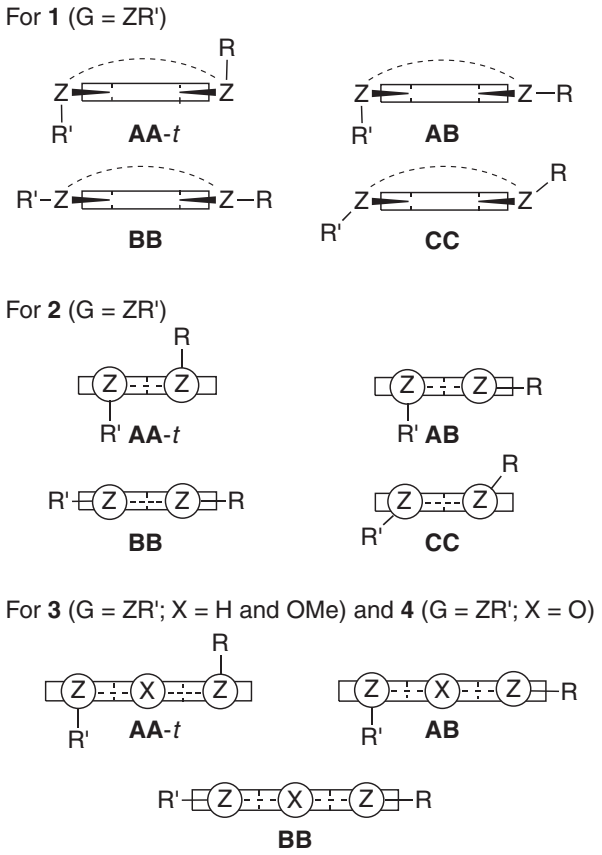

Scheme 3. Typical structures for **1**–**4** with G = ZR′ and X = H, O, and OMe, Together with the interactions.

Here, we discuss factors to control the G···Z distances employing **1**–**4**, containing *r*(Z···Z) in **5**–**7**, to clarify the real course to determine the G···Z distances operating around the G···Z moiety. The consideration will shed light on the causality in weak interactions and the concept must be widely applicable to understand and discuss what happens in weak interactions. Quantum chemical (QC) calculations are employed to support and clarify the causality in weak interactions.

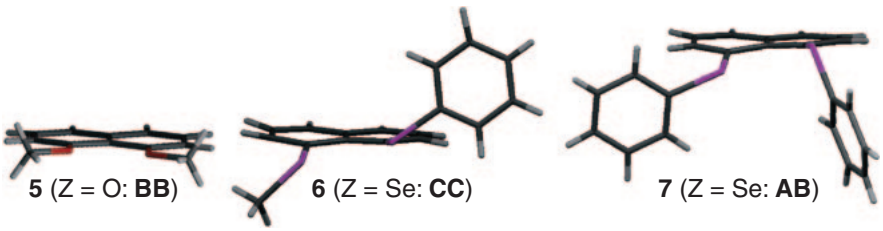

Scheme 4. Structures of **5** (Z = O: **BB**), **6** (Z = Se: **CC**), and **7** (Z = Se: **AB**).

Table 1. Observed and Calculated Non-Bonded r(Z···Z) Distances[a)]

	AA-*t*	AB		CC		BB	Method
5–**7** (Z = O) (3.04 Å[b),c)])							
r_{obsd}[d)]		2.597[e)]	2.616[f)]			2.545[g)]	X-ray
Δr_{obsd}[h)]		−0.44	−0.42			−0.50	X-ray
r_{calcd}[d)]	2.759	2.651				2.530	**5**: MP2[i)]
Δr_{calcd}[j)]	−0.28	−0.39				−0.51	**5**: MP2[i)]
r_{calcd}[d)]	2.758	2.653				2.549	**5**: B3LYP[k)]
Δr_{calcd}[j)]	−0.28	−0.39				−0.49	**5**: B3LYP[k)]
5–**7** (Z = S) (3.60 Å[c),l)])							
r_{obsd}[d)]		3.047[m)]	3.021[n)]	2.927[o)]			X-ray
Δr_{obsd}[h)]		−0.55	−0.58	−0.67			X-ray
r_{calcd}[d)]	3.245	3.059		3.060		2.938	**5**: MP2[i)]
Δr_{calcd}[j)]	−0.36	−0.54		−0.54		−0.66	**5**: MP2[i)]
r_{calcd}[d)]	3.268	3.032		2.937		2.937[p)]	**5**: B3LYP[k)]
Δr_{calcd}[j)]	−0.33	−0.57		−0.66		−0.66[p)]	**5**: B3LYP[k)]
5–**7** (Z = Se) (3.80 Å[c),q)])							
r_{obsd}[d)]		3.135[r)]		3.058[s)]	3.070[t)]		X-ray
Δr_{obsd}[h)]		−0.67		−0.75	−0.73		X-ray
r_{calcd}[d)]	3.396	3.166		3.159		3.058	**5**: MP2[i)]
Δr_{calcd}[j)]	−0.40	−0.63		−0.64		−0.74	**5**: MP2[i)]
r_{calcd}[d)]	3.436	3.155		3.104		3.075[p)]	**5**: B3LYP[k)]
Δr_{calcd}[j)]	−0.36	−0.65		−0.70		−0.73[p)]	**5**: B3LYP[k)]

a) In Å. b) $2r_{vdW}$(O). c) Ref. 30. d) Non-bonded Z···Z distance. e) For **5** (Z = O), Ref. 15. f) For **6** (Z = O), Ref. 17. g) For **7** (Z = O), Ref. 17. h) $\Delta r_{obsd} = r_{obsd} - 2r_{vdW}$(Z). i) Calculations being performed with the MP2/6-311+G(d) method for O, S, and Se and 6-31G(d) method for C and H. j) $\Delta r_{calcd} = r_{calcd} - 2r_{vdW}$(Z). k) Calculations being performed with the B3LYP/6-311+G(2d,p) method. l) $2r_{vdW}$(S). m) For **6** (Z = S), Ref. 17. n) For **7** (Z = S), Refs. 17 and 18. o) For **5** (Z = S), Ref. 16. p) Two imaginary frequencies being given. q) $2r_{vdW}$(Se). r) For **7** (Z = Se), Ref. 17. s) For **5** (Z = Se), Ref. 17. t) For **6** (Z = Se), Refs. 5a, 5c, and 5e.

Computational Methodology

QC calculations are performed on **1** (G = H, ZR = SeMe), **2** (H, SeMe), **5** (Z = O), **5** (Z = S), and **5** (Z = Se). The 6-311+G(d) basis sets are employed for O, S, Se, and halogens and the 6-31G(d) basis sets for C and H in Gaussian 03.[21] Structural optimizations are performed at the Møller–Plesset second-order energy correlation (MP2) level.[22] The compounds are full optimized with the basis set system at the MP2 level. Optimizations are further performed on **1** (H, SeMe) and **2** (H, SeMe) by fixing the torsional angle of $\phi(C_2C_1ZC_R)$ for **1** (H, SeMe) and $\phi(C_{8a}C_1ZC_R)$ for **2** (H, SeMe), employing the Z-matrix. QC calculations are similarly performed on **1** (H, SeMe), **2** (H, SeMe), **5** (Z = O), **5** (Z = S), and **5** (Z = Se) at the density functional theory (DFT) level of the Becke three parameter hybrid functionals with the Lee–Yang–Parr correlation functional (B3LYP)[23] using the 6-311+G(2d,p) basis sets.

Results and Discussion

The observed and calculated structural features in **1**–**4** necessary for discussion are explained exemplified by **5**–**7**. The real course to control the G···Z distances in **1**–**4** will be elucidated based on the results of QC calculations exemplified by **1** (H, SeMe) and **2** (H, SeMe).

Structures of 1,8-Bis(chalcogena)naphthalenes. Three types of structures are observed for **5**–**7** by X-ray crystallographic analysis: **BB** for **5** (Z = O),[15] **CC** for **5** (Z = S),[16] **5**

(Z = Se),[17] **6** (Z = Se),[5a,5c,5e] and **7** (Z = Te),[19] and **AB** for **6** (Z = O),[17] **6** (Z = S),[17] **7** (Z = O),[17] **7** (Z = S),[17,18] and **7** (Z = Se).[17] Scheme 4 illustrates the typical structures for **5** (Z = O: **BB**), **6** (Z = Se: **CC**), and **7** (Z = Se: **AB**).

Table 1 shows the observed r(Z···Z) distances of **5**–**7** (Z = O, S, and Se) and calculated values for **5** (Z = O, S, and Se) at the MP2 and DFT (B3LYP) levels. While three structures, **AA**-*t* (C_2), **AB** (C_1), and **BB** (C_{2v}), are optimized to be stable for **5** (Z = O), three **AA**-*t* (C_2), **AB** (C_1), and **CC** (C_2)[24] are for **5** (Z = S and Se), when optimized at both the MP2 and DFT levels.[20] Although **BB** (C_{2v}) are optimized for each of **5** (Z = S and Se) if calculated assuming C_{2v} symmetry, they correspond to structures with two imaginary frequencies.[20] The ($r_{obsd}, r_{calcd:MP2}, r_{calcd:B3LYP}$) values are (2.545, 2.530, 2.549), (2.927, 3.060, 2.937), and (3.058, 3.159, 3.104) in angstroms for **5** (Z = O: **BB**), **5** (Z = S: **CC**), and **5** (Z = Se: **CC**), respectively. While the differences ($\Delta r = r_{calcd} - r_{obsd}$) seem small for **5** (Z = O: **BB**) (≈0.01 Å), they become larger for **5** (Z = S: **CC**) and **5** (Z = Se: **CC**) (≈0.1 Å).

Observed r(Z···Z) values increase in the order of **BB** < **CC** < **AB**, as a whole, and the calculated values become larger in the order of **BB** < **CC** ≤ **AB** < **AA**-*t*. If the r(Z···Z) values decrease as the Z···Z interactions become stronger, the Z···Z interactions are concluded to be stronger in the order of **AA**-*t* < **AB** ≤ **CC** < **BB**. The order would be acceptable for **AA**-*t* < **AB** ≤ **CC**. However, that of **BB** must not be so strong especially for Z of heavier atoms. The factor to determine the non-bonded r(Z···Z) distances should be examined carefully. The mechanism to control the r(Z···Z) distances must be common for Z = O, S, Se, and Te.

Consideration of these results led us to a hypothesis: the real determinant of the non-bonded r(Z···Z) distances is not the attractive closed-shell Z···Z interactions but the repulsive interactions between Me or Ph and H at the 2- and/or 7-positions (^{2}H and/or ^{7}H) in **5**–**7**. Similarly, the repulsive interaction between R and ^{2}H (or ^{6}H) plays an important role in **1**. The proposed mechanism is suggested to operate to control the Z···Z distances in **1**–**7**. The mechanism is exemplified by the behavior of Me and ^{2}H (or ^{6}H) in **1** (H, SeMe) and that of Me and ^{8}H (or ^{2}H) in **2** (H, SeMe), based on the QC calculations. The case of **1** (H, SeMe) is discussed first.

Repulsive Interaction between Me and ^{2}H in 1 (H, SeMe). QC calculations are performed on **1** (H, SeMe) at the MP2 level. The **A** structure is optimized to be stable with $\phi = 90.12°$ (=$\angle C_2C_1SeC_{Me}$). While **B** is also optimized at $\phi = 0$ and 180°, they are predicted to be the transition states between **A** and the equivalent. QC calculations are further performed with variously fixed ϕ values. The results are collected in Table S1 of the Supporting Information (SI). The plot of the calculated energies (E) versus ϕ for **1** (H, SeMe) is shown in Figure S1 of the SI.

Figure 1 shows the plots of r(Se···^{2}H) (=r_1) and r(Se···^{6}H) (=r_2) versus $\angle C_2C_1SeC_{Me}$ (=ϕ) in **1** (H, SeMe) and Figure 2 exhibits the plots of $\angle C_2C_1Se$ (=θ_1) and $\angle C_6C_1Se$ (=θ_2) versus ϕ in **1** (H, SeMe). The variables for **1** (H, SeMe) are shown in Figure 1. Plots in Figures 1 and 2 are very similar to each other. Consequently, r_1 and r_2 are expected to change monotonically depending on θ_1 and θ_2, respectively. Figure 3 displays the plots of r_1 versus θ_1 and r_2 versus θ_2 in **1** (H, SeMe), where the x-axis is used commonly for θ_1 and θ_2. The results demonstrate that r_1 and r_2 change linearly depending on θ_1 and θ_2, respectively. Namely, r_1 and r_2 change depending on ϕ through θ_1 and θ_2. The repulsive interaction between Me and ^{2}H is largest at $\phi \approx 0°$ whereas it is smallest when $\phi \approx 180°$. The interaction between Me and ^{6}H is smallest at $\phi \approx 0°$ whereas it is largest at $\phi \approx 180°$. The two repulsions are balanced at $\phi \approx 90°$. The r(Se···^{2}H) (=r_1) and r(Se···^{6}H) (=r_2) distances are demonstrated to change by the repulsive interaction between Me and ^{2}H in **1** (H, SeMe): r_1 and r_2 are controlled by the repulsive interaction between Me and ^{2}H (and ^{6}H), as expected.

The repulsive interaction between Me and ^{2}H (and ^{6}H) is well established to play an important role to control r_1 and r_2 in **1** (H, SeMe). The factor to control the non-bonded Z···Z distances in **5**–**7** is similarly investigated exemplified by **2** (H,

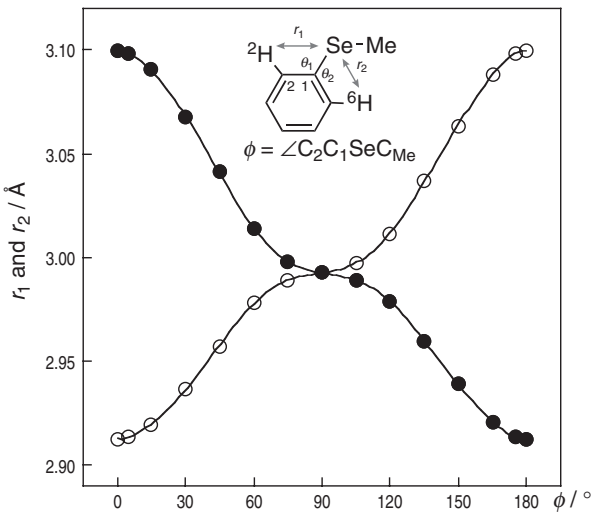

Figure 1. Plots of r_1 (●) and r_2 (○) versus ϕ in **1** (H, SeMe), calculated at the MP2 level.

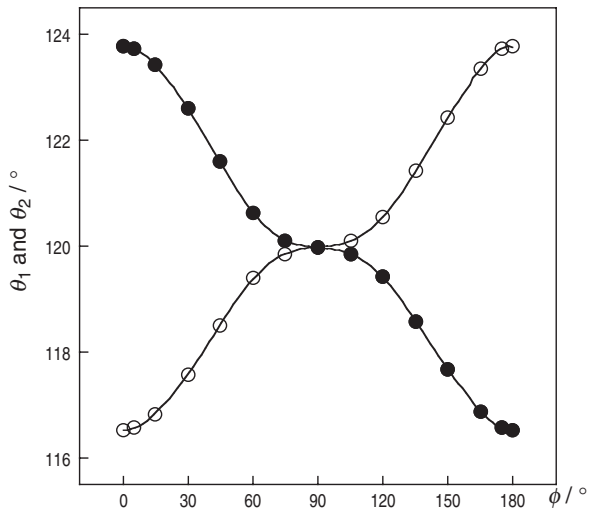

Figure 2. Plots of θ_1 (●) and θ_2 (○) versus ϕ in **1** (H, SeMe), calculated at the MP2 level.

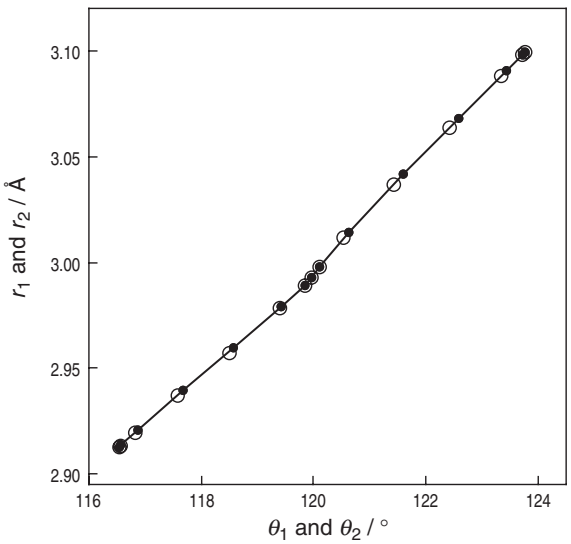

Figure 3. Plots of r_1 versus θ_1 (●) and r_2 versus θ_2 (○) in **1** (H, SeMe), calculated at the MP2 level.

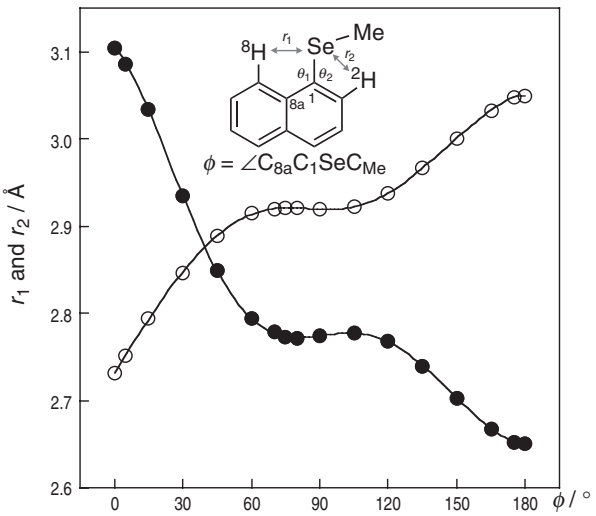

Figure 4. Plots r_1 (●) and r_2 (○) versus ϕ in **2** (H, SeMe), calculated at the MP2.

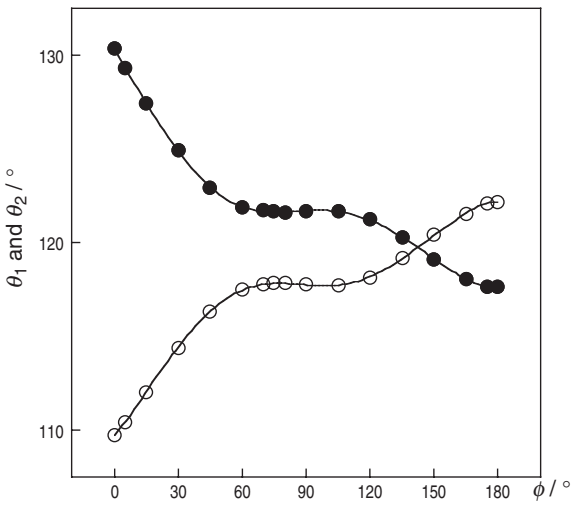

Figure 5. Plots θ_1 (●) and θ_2 (○) versus ϕ in **2** (H, SeMe), calculated at the MP2 level.

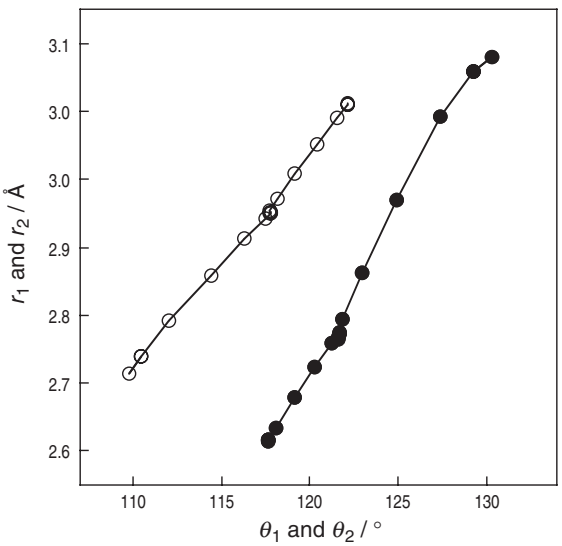

Figure 6. Plots of r_1 versus θ_1 (●) and r_2 versus θ_2 (○) in **2** (H, SeMe), calculated at the MP2 level.

SeMe), where **2** (H, SeMe) is not symmetric in respect to the SeMe group.

Repulsive Interaction between Me and ^{2}H in 2 (H, SeMe). The **A** structure is optimized to be stable for **2** (H, SeMe) ($\phi = 75.03°$) at the MP2 level of calculations. While **B′** ($\phi = 0°$) and **B** ($\phi = 180°$) are also optimized, both of them are predicted to be unstable at the MP2 level. **B** and **B′** are predicted to be the transition states between **A** and the equivalent. QC calculations are further performed on **2** (H, SeMe) with variously fixed torsional angles of $C_{8a}C_1SeC_{Me}$ ($=\phi$). The results are collected in Table S2 of the SI[25] and the plot of energy (E) versus ϕ for **2** (H, SeMe) is shown in Figure S2 of the SI.

Figure 4 exhibits the plots of r(Se···^{8}H) ($=r_1$) and r(Se···^{2}H) ($=r_2$) versus $\angle C_{8a}C_1SeC_{Me}$ ($=\phi$) and Figure 5 shows the plots of $\angle C_{8a}C_1Se$ ($=\theta_1$) and $\angle C_2C_1Se$ ($=\theta_2$) versus ϕ in **2** (H, SeMe). The variables for **2** (H, SeMe) are shown in Figure 4. The figures are similar. Figure 6 displays the plots of r_1 versus θ_1 and r_2 versus θ_2 in **2** (H, SeMe), where the x-axis is used commonly for θ_1 and θ_2, similarly to the case of Figure 3. The r_1 and r_2 values are shown to change almost linearly depending on θ_1 and θ_2, respectively, although the ranges are not the same. They change depending on ϕ through θ. The r_1 and r_2 values are demonstrated to be really controlled by the repulsive interaction between Me and ^{2}H (and ^{8}H) in **2** (H, SeMe).

While plots in Figures 1–3 are symmetric, those in Figures 4–6 are not, which is the reflection of the geometric difference between **1** (H, SeMe) and **2** (H, SeMe). While **1** (H, SeMe) is optimized at $\phi = 90.12°$ ($=\angle C_2C_1SeC_{Me}$) (C_s symmetry), **2** (H, SeMe) is at $\phi = 75.03°$ ($=\angle C_{8a}C_1SeC_{Me}$) ($C_1$ symmetry).

The importance of the closed-shell repulsive interaction between Me and ^{8}H (and ^{2}H) in **2** (H, SeMe) is well established

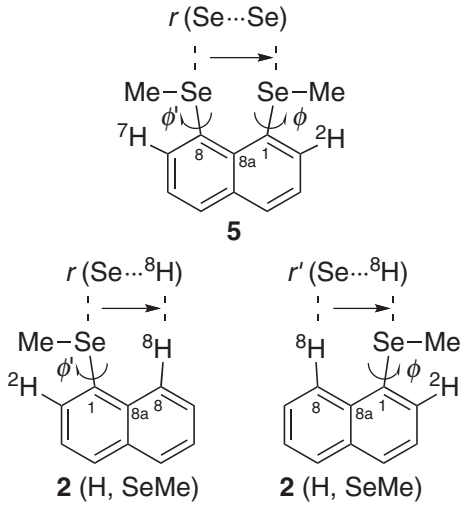

Scheme 5. Correlation between r(Se···Se) in **5** (Z = Se) and r(Se···^{8}H) and r'(Se···^{8}H) in **2** (H, SeMe).

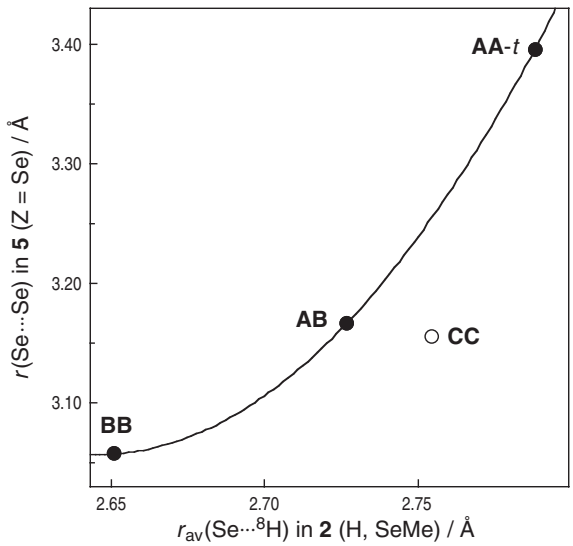

Figure 7. Plot of optimized r(Se···Se) in **5** (Z = Se) versus r_{av}(Se···^{8}H) in **2** (H, SeMe).

Table 2. Optimized r(Se···Se), $\angle C_{8a}C_1Se_1C_{Me}$ (ϕ), $\angle C_{8a}C_8Se_8C_{Me}$ (ϕ'), and $\angle Se_1C_1C_8Se_8$ (ϕ'') for **AA**-*t*, **AB**, **CC**, and **BB** in **5** (Z = Se), Together with r(Se···^{8}H), r'(Se···^{8}H), and r_{av}(Se···^{8}H) in **2** (H, SeMe) at ϕ and ϕ'

	5 (Z = Se)				**2** (H, SeMe)		
	r(Se···Se)/Å	ϕ/°	ϕ'/°	ϕ''/°	r(Se···^{8}H)/Å	r'(Se···^{8}H)/Å	r_{av}(Se···^{8}H)/Å
AA-*t*	3.3958	64.12	64.12	24.48	2.7880	2.7880	2.7880
AB	3.1664	73.75	160.42	28.10	2.7746[a)]	2.6786[b)]	2.7266
CC	3.1557	126.91	126.91	30.84	2.7545	2.7545	2.7545
BB	3.0575	180.00	180.00	0.00	2.6510	2.6510	2.6510

a) At ϕ = 73.75° (**A**). b) At ϕ = 160.42° (**B**).

to control the r_1 and r_2 values. The next extension is to explain the r(Se···Se) values in **5** (Z = Se) based on the r(Se···H) values in **2** (H, SeMe).

Analysis of r(Se···Se) in 5 Based on r(Se···^{8}H) in 2. An r(Se···Se) value in **5** (Z = Se) is expected to correlate to the r(Se···^{8}H) and r'(Se···^{8}H) values in **2** (H, SeMe) which are evaluated at ϕ($C_{8a}C_1Se_1C_{Me}$) and ϕ'($C_{8a}C_8Se_8C_{Me}$) in **5** (Z = Se): ϕ and ϕ' correspond to those in **AA**-*t*, **AB**, **CC**, and **BB**. Scheme 5 explains the correlation between r(Se···Se) in **5** (Z = Se) and r(Se···^{8}H) and r'(Se···^{8}H) in **2** (H, SeMe), where the hypothetical r(Se···^{8}H) and r'(Se···^{8}H) values in **2** (H, SeMe) are calculated using ϕ and ϕ' in **5** (Z = Se), respectively.

Table 2 collects the optimized ϕ and ϕ' values for **AA**-*t*, **AB**, **CC**, and **BB** in **5** (Z = Se), together with r(Se···Se). The steric repulsion between Se–Me and ^{2}H in **2** (H, SeMe) at ϕ and ϕ' must be reflected in the r(Se···^{8}H) and r'(Se···^{8}H) distances under the conditions. Consequently, the r(Se···^{8}H) + r'(Se···^{8}H) value will contain the steric repulsion between Se–Me and ^{2}H at both ϕ and ϕ' in **2** (H, SeMe). The hypothetical r(Se···^{8}H) and r'(Se···^{8}H) values are calculated assuming ϕ and ϕ' for **2** (H, SeMe) and the correlation between r(Se···Se) in **5** (Z = Se) and r(Se···^{8}H) + r'(Se···^{8}H) in **2** (H, SeMe) is examined. The r_{av}(Se···^{8}H) value [=(r(Se···^{8}H) + r'(Se···^{8}H))/2] is employed in the analysis, since r(Se···^{8}H) + r'(Se···^{8}H) reaches nearly twice the value of r(Se···Se). The relations between r(Se···^{8}H) and ϕ shown in Figure 4 are employed in the calculations. The results are also collected in Table 2. The r(Se···Se) values for **AA**-*t*, **AB**, **CC**, and **BB** in **5** (Z = Se) are assumed to be correlated to the averaged values at ϕ and ϕ' [r_{av}(Se···^{8}H) = (r(Se···^{8}H) + r'(Se···^{8}H))/2] in **2** (H, SeMe). Table 2 also lists the r(Se···^{8}H), r'(Se···^{8}H), and r_{av}(Se···^{8}H) values in **2** (H, SeMe).

How is the correlation between r(Se···Se) and r_{av}(Se···^{8}H)? The r(Se···Se) values in **5** (Z = Se) are plotted versus r_{av}(Se···^{8}H) estimated for **2** (H, SeMe). Figure 7 shows the results. The r(Se···Se) values correlate well with r_{av}(Se···^{8}H) as a whole. Data for **CC** deviate negatively from the correlation curve, if the correlation curve is drawn for the data of **AA**-*t*, **AB**, and **BB**. Why do data for **CC** deviate? The deviation could come from the deformation in naphthalene ring. The deformation results in the flipping of the C–Se bonds from the top or bottom of the naphthyl plane in **5** (Z = Se). Such deformation can be estimated by the torsional angle of ϕ'' (=$\angle Se_1C_1C_8Se_8$). Table 2 also contains the ϕ''($Se_1C_1C_8Se_8$) values for **AA**-*t*, **AB**, **CC**, and **BB** in **5** (Z = Se). The value is largest for **CC** of **5** (Z = Se). The deformation will operate to avoid the severe repulsion between the Se···Se atoms in **5** (Z = Se: **CC**). As shown in Figure 7, r(Se···Se) in **5** (Z = Se: **CC**) is shorter than that predicted from the correlation curve

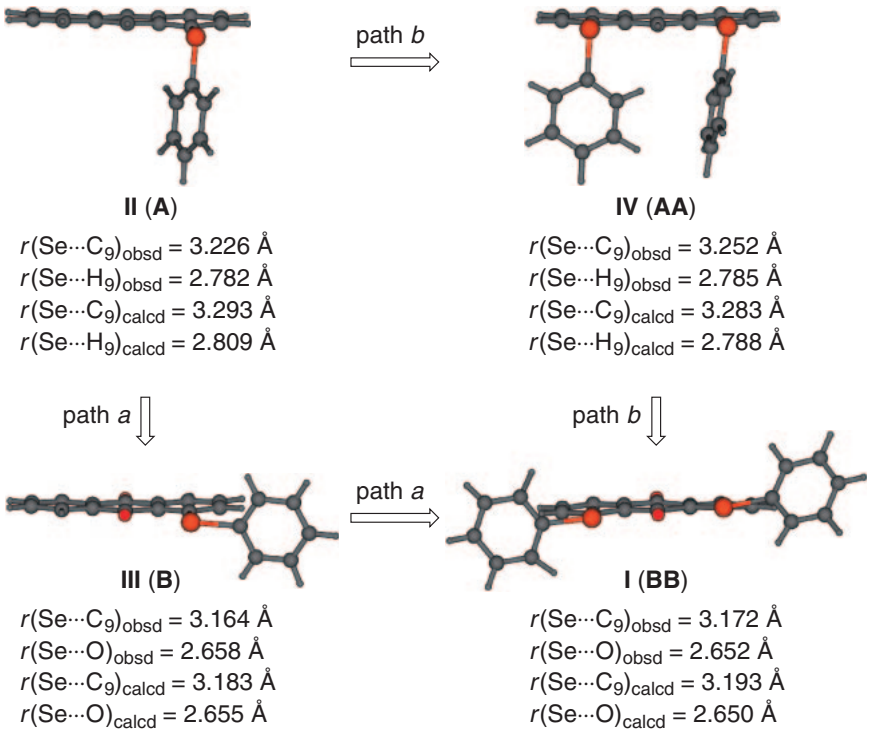

Scheme 6. Change in r(Se···C_9) in the formation of C_2Se_2O 5c–6e in **I** (**BB**) starting from n_p(Se) 1c–2e in **II** (**A**).

based on **2** (H, SeMe). The correlation between r(Se···Se) and r_{av}(Se···^{8}H) containing the deviation of the data for **5** (Z = Se: **CC**) can be well explained by considering the deformation, since such deformation must be very small in **2** (H, SeMe).

The factor to control r(Se···Se) in **5** (Z = Se) is well explained based on the repulsive interaction between Me and ^{8}H (and ^{2}H) in **2** (H, SeMe). The Se···Se interaction cannot be the main factor to determine the non-bonded Se···Se distance at the 1,8-positions of **5** (Z = Se), although the interaction could be attractive in some cases.[26] The shorter r(Z···Z) value in **CC**, relative to that in **AB**, is also observed for Z = O and S, when calculated at the MP2 level.

The closed-shell Z···Z interactions between π(Ar) (or C_i) and ^{2}H in the aryl derivatives of **2** also give rise to similar repulsion, which must also control the non-bonded r(Z···Z) distances. The applicability of the concept for the non-bonded distances in aryl derivatives is examined next.

Factors to Control *r*(G···Se) Values. Scheme 6 illustrates the structures appeared in the formation of 1,8-bis(phenylselanyl)anthraquinone **I** (**4**: G = ZR = SePh) starting from 1-(phenylselanyl)anthracene **II** (**3**: G = H; ZR = SePh). The process contains the formation of extended hypervalent C_2Se_2O 5c–6e interactions of the σ^*(C–Se)←n_p(O)→σ^*(Se–C) type in **I** (**BB**)[13] from n_p(Se) (1c–2e) in **II** (**A**).[27] A process via 1-(phenylselanyl)anthraquinone [**III** (**B**) (**4**: G = H; ZR = SePh)] with the formation of CSeO 3c–4e[28] of the σ^*(C–Se)←n_p(O) type is called path a and another one via 1,8-bis(phenylselanyl)anthracene [**IV** (**AA**) (**3**: G = ZR = SePh)] with two independent n_p(Se) (1c–2e) is named path b.[13]

How are the non-bonded distances at the 1,8,9-positions changed in the processes? The r(Se···C_9) values are employed for the discussion. The observed and calculated r(Se···C_9) values are given in Scheme 6, together with r(Se···G) values.[29] The calculated and observed r(Se···C_9) values are shown to decrease in the order of **II** (**A**) ≈ **IV** (**AA**) > **III** (**B**) ≈ **I** (**BB**). The results are also well explained by the repulsion mechanism.

A considerable number of observed and calculated non-bonded r(G···Z) values are reported hitherto. Table 3 displays the r(G···Z) values at the benzene 1,2- and naphthalene 1,8-positions suitable for the discussion. Table 4 summarizes those at the anthracene 1,8,9- and anthraquinone 1,8,9-positions. Based on the r(G···Z) values shown in Tables 3 and 4, the non-bonded r(G···Z) distances are confirmed to be smaller in the order of r(**AA**-*t*) > r(**AB**) ≥ r(**CC**) > r(**BB**). The results demonstrate that the non-bonded r(G···Z) distances are not controlled by the G···Z interactions but by the repulsive interactions between R_Z and H at the backside of G.

Conclusion

Weak interactions control fine structures of molecules and create high functionalities of materials. However, it is still difficult to demonstrate the causality of phenomena arising from weak interactions, since weak interactions usually operate behind other factors of superficial contributions. Observed phenomena in weak interactions should be analyzed by a simple syllogism, similarly to the case of strong interactions. However, mechanisms operating in weak interactions are sometimes quite different from those in strong interactions. Factors to control the non-bonded G···Z distances are analyzed as a typical case for the causality of weak interactions.

Observed and/or calculated r(Z···Z) values at benzene 1,2-, naphthalene 1,8-, and anthracene/anthraquinone 1,8,9-posi-

Table 3. Observed and Calculated Non-Bonded G···Z Distances in Benzene 1,2- and Naphthalene 1,8-Positions[a)]

Compound (G, Z)[b)]	**AA**-*t*	**AB**	**CC**	**BB**
Observed				
Benzene 1,2-positions				
1 (OR, OR′)	2.729[c)]	2.687[d)]		2.587[e)]
	117.71, 120.13[f)]	120.27, 115.85[f)]		115.14, 115.95[f)]
1 (SR, SR′)	3.304[g)]	3.134[h)]		3.003[i)]
	122.12, 122.12[f)]	120.86, 117.71[f)]		116.54, 117.15[f)]
Naphthalene 1,8-positions				
2 (OR, OR′)		2.604[j)]		2.547[k)]
		119.75, 116.38[f)]		117.29, 117.29[f)]
2 (SR, SR′)		3.047[l)]	2.918[m)]	
		124.65, 121.56[f)]	121.10, 122.50[f)]	
2 (SeR, SeR′)		3.135[n)]	3.051[o)]	
		123.39, 122.63[f)]	122.93, 123.89[f)]	
2 (TeR, TeR′)		3.287[p)]		
		123.27, 115.89[f)]		
Calculated				
Benzene 1,2-positions				
1 (OMe, OMe)[q)]	2.830	2.726		2.591
1 (SeMe, SeMe)[q)]	3.579	3.332		3.259
Naphthalene 1,8-positions				
2 (OMe, OMe)[r)]	2.759	2.651		2.530
2 (SMe, SMe)[r)]	3.245	3.059	3.060	2.938
2 (SeMe, SeMe)[r)]	3.396	3.166	3.159	3.058

a) In Å. b) **1** (^{2}G, ^{1}ZR) and **2** (^{8}G, ^{1}ZR). c) 1,2-Bis(*o*-nitrophenoxy)benzene: Ref. 31. d) 2,2′-Dimethoxydiphenyl ether: Ref. 32. e) 1,2-Dimethoxybenzene: Ref. 33. f) Angles θ_1 and θ_2. g) 1,2-Bis(*o*-nitrophenylthio)benzene: Ref. 34. h) 1,2-Bis[*o*-(phenylthio)phenylthio]benzene: Ref. 35. i) 1,2-Bis(methylthio)benzene: Ref. 36. j) 1-Methoxy-8-phenoxynaphthalene: Ref. 17. k) 1,8-Dimethoxynaphthalene: Ref. 15. l) 1-Methylthio-8-(phenylthio)naphthalene: Ref. 17. m) 1,8-Bis(methylthio)naphthalene: Ref. 16. n) 1,8-Bis(phenylselanyl)naphthalene: Ref. 17. o) 1-Methylselanyl-8-(phenylselanyl)naphthalene: Refs. 5c and 5e. p) 1,8-Bis(phenyltelluro)naphthalene: Ref. 19. q) Calculations being performed with the B3LYP/6-311+G(2d,p) method. r) Calculations being performed with the MP2/6-311+G(d) method for O, S, and Se and 6-31G(d) method for C and H.

tions increase in an order of **BB** < **CC** ≤ **AB** < **AA**-*t*, as a whole. If the *r*(Z···Z) values at the positions decrease as the closed-shell Z···Z interactions become stronger, the Z···Z interactions are concluded to be stronger in an order of **AA**-*t* < **AB** ≤ **CC** < **BB**. The order could be acceptable for **AA**-*t* < **AB** ≤ **CC**. The mechanism for **BB** is unlikely, since the **BB** interaction must not be so strong especially for Z of heavier atoms. By careful examination of the mechanism based on QC calculations on **1** (H, SeMe) and **2** (H, SeMe), the non-bonded Z···Z distances are demonstrated to be controlled not by the closed-shell G···Z interaction but by the repulsive interaction between R and ^{2}H in 1,8-$(RZ)_2C_{10}H_6$, for example. The proposed mechanism is shown to explain the observed and calculated *r*(Z···Z) values at benzene 1,2-, naphthalene 1,8-, and anthracene/anthraquinone 1,8,9-positions. The proposed mechanism and idea will help us to analyze the weak interactions.

This work was supported by a Grant-in-Aid for Scientific Research on Priority Areas (A) (Nos. 11166246, 12042259, 16550038, and 1950041) from the Ministry of Education, Culture, Sports, Science and Technology, Japan, by a Grant-in-Aid for Encouragement of Young scientists (No. 13740354) from Japan Society for Promotion of Science, and by the Hayashi Memorial Foundation for Female Natural Scientists.

Supporting Information

Optimized structures for **1** (H, SeMe) and **2** (H, SeMe) with variously fixed torsional angles of $C_2C_1SeC_{Me}$ and $C_{8a}C_1SeC_{Me}$ (=ϕ), respectively; plot of *E* versus ϕ in **1** (H, SeMe) with the MP2/6-311+G(d) method: plots of *E* versus ϕ and θ_1 and θ_2 versus ϕ in **2** (H, SeMe) with the MP2/6-311+G(d) and B3LYP/6-311+G(d) methods; optimized structures given by Cartesian coordinates for examined compounds. These materials are available free of charge on the web at http://www.csj.jp/journals/bcsj/.

Table 4. Observed and Calculated Non-Bonded G···Z Distances in Anthracene 1,8,9- and Anthraquinone 1,8,9-Positions[a)]

Compound (G, Z)[b)]	**AA**-*t*	**AB**	**BB**
Observed			
Anthracene 1,8,9-positions			
3 (G, OMe)		2.568[c),d)]	2.420[d),e)]
		117.26, 115.43[f)]	125.15, 114.27[f)]
3 (G, SePh)	2.774[g),h)]	2.731[i),j)]	
	120.84, 117.86[f)]	122.57, 117.57[f)]	
Anthraquinone 1,8,9-positions			
4 (O(sp), OR)			2.618[k),l)]
			121.52, 119.69[f)]
			2.634[l),m)]
			120.79, 120.43[f)]
4 (O(sp), SR)			2.650[l),n)]
			121.22, 119.35[f)]
			2.636[l),o)]
			120.47, 120.80[f)]
4 (O(sp), SeR)			2.661[l),p)]
			120.85, 120.39[f)]
			2.617[l),q)]
			122.57, 117.57[f)]
Calculated			
Anthracene 1,8,9-positions			
3 (OMe, OMe)[r)]		2.578[d),s)]	
3 (G, SMe)[r)]	2.788[t),u)]	2.714[v),w)]	
3 (G, SeMe)[r)]	3.055[x),y)]	2.765[z),aa)]	
Anthraquinone 1,8,9-positions			
4 (O(sp), OMe)[r)]			2.578[l),m)]
4 (O(sp), SMe)[r)]			2.626[l),o)]
4 (O(sp), SeMe)[r)]			2.649[l),q)]

a) In Å. b) **3** (^{9}G, ^{1}ZR) and **4** (^{9}G, ^{1}ZR). c) 1,8-Dimethoxy-9-(trifluoromethanesulfonyloxy)anthracene: Ref. 37. d) MeO groups at 1,8-positions: type **B**. e) 1,8-Dimethoxyanthracene: Ref. 38. f) Angles θ_1 and θ_2. g) 1,8-Bis(phenylselanyl)anthracene: Ref. 13. h) PhSe groups at 1,8-positions: type **A**. i) 9-Methoxy-1,8-bis(phenylselanyl)anthracene: Ref. 13. j) PhSe groups at 1,8-positions: type **B**. k) 1-(3-Pentynyloxy)anthraquinone: Ref. 39. l) Type **B**. m) 1,8-Dimethoxyanthraquinone: Ref. 14. n) 1-(6-Mercaptohexylthio)anthraquinone: Ref. 40. o) 1,8-Bis(methylthio)anthraquinone: Ref. 14. p) 1-(Phenylselanyl)-anthraquinone: Ref. 28. q) 1,8-Bis(methylselanyl)anthraquinone: Ref. 14. r) Calculations being performed with the B3LYP/6-311+G(2df) method for O, S, and Se and 6-311+G(2d,p) method for C and H. s) 1,8,9-Trimethoxyanthracene: Ref. 14. t) 1,8-Bis(methylthio)anthracene. u) MeS groups at 1,8-positions: type **A**. v) 9-Methoxy-1,8-bis(methylthio)anthracene. w) MeS groups at 1,8-positions: type **B**. x) 1,8-Bis(methylselanyl)anthracene: Ref. 14. y) MeSe groups at 1,8-positions: type **A**. z) 9-Methoxy-1,8-bis(methylselanyl)anthracene: Ref. 14. aa) MeSe groups at 1,8-positions: type **B**.

References

1 a) *Molecular Interactions: From van der Waals to Strongly Bound Complexes*, ed. by S. Scheiner, Wiley, New York, **1997**. b) K. Müller-Dethlefs, P. Hobza, *Chem. Rev.* **2000**, *100*, 143. c) B. Brutschy, P. Hobza, *Chem. Rev.* **2000**, *100*, 3861; U. Buck, F. Huisken, *Chem. Rev.* **2000**, *100*, 3863; B. Brutschy, *Chem. Rev.* **2000**, *100*, 3891; H. J. Neusser, K. Siglow, *Chem. Rev.* **2000**, *100*, 3921; C. Desfrançois, S. Carles, J. P. Schermann, *Chem. Rev.* **2000**, *100*, 3943; E. J. Bieske, O. Dopfer, *Chem. Rev.* **2000**, *100*, 3963; C. E. H. Dessent, K. Müller-Dethlefs, *Chem. Rev.* **2000**, *100*, 3999; C. Dedonder-Lardeux, G. Grégoire, C. Jouvet, S. Martrenchard, D. Solgadi, *Chem. Rev.* **2000**, *100*, 4023; Q. Zhong, A. W. Castleman, Jr., *Chem. Rev.* **2000**, *100*, 4039; G. Niedner-Schatteburg, V. E. Bodybey, *Chem. Rev.* **2000**, *100*, 4059; O. Engkvist, P.-O. Åstrand, G. Karlström, *Chem. Rev.* **2000**, *100*, 4087; P. E. S. Wormer, A. van der Avoird, *Chem. Rev.* **2000**, *100*, 4109; K. S. Kim, P. Tarakeshwar, J. Y. Lee, *Chem. Rev.* **2000**, *100*, 4145; M. Orozco, F. J. Luque, *Chem. Rev.* **2000**, *100*, 4187; G. Chałasiński, M. M. Szczęśniak, *Chem. Rev.* **2000**, *100*, 4227; P. Hobza, Z. Havlas, *Chem. Rev.* **2000**, *100*, 4253.

2 Let us consider a molecular complex (MC) formation from

a selenide with iodine, $O(CH_2CH_2)_2Se\cdots I–I$, as an example.[3] The attractive interaction between Se and I_2 and the formation of the Se···I bond correspond to cause **1** and result **A**, respectively. The Se···I distance should be shorter than the sum of van der Waals radii of the atoms but longer than the sum of covalent radii of the atoms: the observed r(Se···I), $r_{vdW}(Se) + r_{vdW}(I)$, and $r_{CO}(Se) + r_{CO}(I)$ are 2.755, 4.15, and 2.50 Å, respectively.[3] Therefore, result **A** is well explained by cause **1**. Result **A** derives spontaneously from cause-**S1**, which produces some phenomena. The I–I distance in the adduct must be smaller than that of the I_2 molecule, which should be result-**R2**. The r(I–I) in the adduct and I_2 itself are 2.956 and 2.666 Å,[3] respectively. Result-**R2** is also well explained by cause **A**.

3 H. Maddox, J. D. McCullough, *Inorg. Chem.* **1966**, *5*, 522.

4 Interactions are defined by the AIM (Atoms-in-Molecules) functions at bond critical points (BCPs: $\boldsymbol{r}_c$).[41,42] They are called closed-shell (CS) interactions when the Laplacian of electron densities at $\boldsymbol{r}_c$ ($\Delta\rho_b(\boldsymbol{r}_c)$) are positive ($\Delta\rho_b(\boldsymbol{r}_c) > 0$) where $\rho_b(\boldsymbol{r}_c)$ are locally depleted relative to the average distribution around $\boldsymbol{r}_c$. On the other hand, $\rho_b(\boldsymbol{r}_c)$ are locally concentrated relative to the average distribution around bond critical points if $\Delta\rho_b(\boldsymbol{r}_c) < 0$. Interactions in this region are called shared-shell (SS) interactions. Interactions of $\Delta\rho_b(\boldsymbol{r}_c) > 0$ are discussed here.

5 a) W. Nakanishi, S. Hayashi, S. Toyota, *Chem. Commun.* **1996**, 371. b) W. Nakanishi, S. Hayashi, H. Yamaguchi, *Chem. Lett.* **1996**, 947. c) W. Nakanishi, S. Hayashi, S. Toyota, *J. Org. Chem.* **1998**, *63*, 8790. d) S. Hayashi, W. Nakanishi, *J. Org. Chem.* **1999**, *64*, 6688. e) W. Nakanishi, S. Hayashi, T. Uehara, *J. Phys. Chem. A* **1999**, *103*, 9906. f) W. Nakanishi, S. Hayashi, *J. Org. Chem.* **2002**, *67*, 38. g) W. Nakanishi, S. Hayashi, T. Arai, *Chem. Commun.* **2002**, 2416. h) W. Nakanishi, S. Hayashi, A. Sakaue, G. Ono, Y. Kawada, *J. Am. Chem. Soc.* **1998**, *120*, 3635. i) S. Hayashi, H. Wada, T. Ueno, W. Nakanishi, *J. Org. Chem.* **2006**, *71*, 5574.

6 H. Margenau, *Phys. Rev.* **1939**, *56*, 1000; H. Margenau, *Phys. Rev.* **1943**, *64*, 131; J. O. Hirschfelder, J. W. Linnett, *J. Chem. Phys.* **1950**, *18*, 130; N. Moore, *J. Chem. Phys.* **1960**, *33*, 471; A. Van der Avoird, *Chem. Phys. Lett.* **1967**, *1*, 24.

7 a) K. D. Asmus, *Acc. Chem. Res.* **1979**, *12*, 436. b) W. K. Musker, *Acc. Chem. Res.* **1980**, *13*, 200. c) A. Kucsman, I. Kapovits, *Non-Bonded Sulfur-Oxygen Interaction in Organic Sulfur Compounds* in *Organic Sulfur Compounds in Organic Sulfur Chemistry: Theoretical and Experimental Advances*, ed. by F. Bernardi, I. G. Csizmadia, A. Mangini, Elsevier, Amsterdam, **1985**, Chap. 4.

8 K. Yamane, S. Hayashi, W. Nakanishi, T. Sasamori, N. Tokitoh, *Polyhedron* **2008**, *27*, 3557.

9 a) L. Pauling, *J. Am. Chem. Soc.* **1947**, *69*, 542. b) L. Pauling, *The Nature of the Chemical Bond*, 3rd ed., Cornell University Press, Ithaca, New York, **1960**, Chap. 7.

10 The formation of iodine adducts with selenides is a typical example: see: O. Hassel, K. O. Strømme, *Acta Chem. Scand.* **1959**, *13*, 1775; O. Hassel, J. Hvoslef, *Acta Chem. Scand.* **1954**, *8*, 873.

11 a) W. Nakanishi, S. Hayashi, H. Kihara, *J. Org. Chem.* **1999**, *64*, 2630. b) W. Nakanishi, S. Hayashi, T. Uehara, *Eur. J. Org. Chem.* **2001**, 3933.

12 a) G. Gafner, *Acta Crystallogr.* **1962**, *15*, 1081. b) M. A. Davydova, Yu. T. Struchkow, *Zh. Strukt. Khim.* **1962**, *3*, 184. c) M. A. Davydova, Yu. T. Struchkow, *Zh. Strukt. Khim.* **1968**, *9*, 1968. d) H. Bock, M. Sievert, Z. Havlas, *Chem.—Eur. J.* **1998**, *4*, 677. e) R. D. Jackson, S. James, A. G. Orpen, P. G. Pringle, *J. Organomet. Chem.* **1993**, *458*, C3.

13 a) W. Nakanishi, S. Hayashi, N. Itoh, *Chem. Commun.* **2003**, 124. b) W. Nakanishi, S. Hayashi, N. Itoh, *J. Org. Chem.* **2004**, *69*, 1676. c) W. Nakanishi, S. Hayashi, T. Furuta, N. Itoh, Y. Nishina, M. Yamashita, Y. Yamamoto, *Phosphorus, Sulfur Silicon Relat. Elem.* **2005**, *180*, 1351.

14 W. Nakanishi, T. Nakamoto, S. Hayashi, T. Sasamori, N. Tokitoh, *Chem.—Eur. J.* **2007**, *13*, 255.

15 R. Cosmo, T. W. Hambley, S. Sternhell, *Acta Crystallogr., Sect. B* **1990**, *46*, 557.

16 R. S. Glass, S. W. Andruski, J. L. Broeker, H. Firouzabadi, L. K. Steffen, G. S. Wilson, *J. Am. Chem. Soc.* **1989**, *111*, 4036.

17 S. Hayashi, W. Nakanishi, *Bull. Chem. Soc. Jpn.* **2008**, *81*, 1605.

18 P. Nagy, D. Szabó, I. Kapovits, A. Kucsman, G. Argay, A. Kálmán, *J. Mol. Struct.* **2002**, *606*, 61, and W. Nakanishi, S. Hayashi, reexamined.[17]

19 H. Fujihara, H. Ishitani, Y. Takaguchi, N. Furukawa, *Chem. Lett.* **1995**, 571.

20 Extended hypervalent 4c–6e interactions of the G···Z–Z···G type are also observed in the linear S_4 and Se_4 atoms.[5a–5d,5g]

21 M. J. Frisch, G. W. Trucks, H. B. Schlegel, G. E. Scuseria, M. A. Robb, J. R. Cheeseman, J. A. Montgomery, Jr., T. Vreven, K. N. Kudin, J. C. Burant, J. M. Millam, S. S. Iyengar, J. Tomasi, V. Barone, B. Mennucci, M. Cossi, G. Scalmani, N. Rega, G. A. Petersson, H. Nakatsuji, M. Hada, M. Ehara, K. Toyota, R. Fukuda, J. Hasegawa, M. Ishida, T. Nakajima, Y. Honda, O. Kitao, H. Nakai, M. Klene, X. Li, J. E. Knox, H. P. Hratchian, J. B. Cross, V. Bakken, C. Adamo, J. Jaramillo, R. Gomperts, R. E. Stratmann, O. Yazyev, A. J. Austin, R. Cammi, C. Pomelli, J. W. Ochterski, P. Y. Ayala, K. Morokuma, G. A. Voth, P. Salvador, J. J. Dannenberg, V. G. Zakrzewski, S. Dapprich, A. D. Daniels, M. C. Strain, O. Farkas, D. K. Malick, A. D. Rabuck, K. Raghavachari, J. B. Foresman, J. V. Ortiz, Q. Cui, A. G. Baboul, S. Clifford, J. Cioslowski, B. B. Stefanov, G. Liu, A. Liashenko, P. Piskorz, I. Komaromi, R. L. Martin, D. J. Fox, T. Keith, M. A. Al-Laham, C. Y. Peng, A. Nanayakkara, M. Challacombe, P. M. W. Gill, B. Johnson, W. Chen, M. W. Wong, C. Gonzalez, J. A. Pople, *Gaussian 03, Revision D.02*, Gaussian, Inc., Wallingford CT, **2004**.

22 C. Møller, M. S. Plesset, *Phys. Rev.* **1934**, *46*, 618; J. Gauss, *J. Chem. Phys.* **1993**, *99*, 3629; J. Gauss, *Ber. Bunsen-Ges. Phys. Chem* **1995**, *99*, 1001.

23 a) A. D. Becke, *Phys. Rev. A* **1988**, *38*, 3098; A. D. Becke, *J. Chem. Phys.* **1993**, *98*, 5648. b) C. Lee, W. Yang, R. G. Parr, *Phys. Rev. B* **1988**, *37*, 785; B. Miehlich, A. Savin, H. Stoll, H. Preuss, *Chem. Phys. Lett.* **1989**, *157*, 200.

24 Although **CC** (C_2) is the desirable structure for **2** (SeMe, SeMe), the structure gives one negative (imaginary) frequency for an internal motion after the frequency analysis. Instead, **2** (SeMe, SeMe) (**CC**: C_1), which is very close to **2** (SeMe, SeMe) (**CC**: C_2), gave positive frequencies for all internal motions by the frequency analysis.

25 See the SI for the results of B3LYP calculations.

26 Similarly, three types of fine structures are observed for 1-methylselanyl-8-(*p*-substituted phenylselanyl)naphthalenes [1-MeSe-8-(*p*-YC_6H_4Se)$C_{10}H_6$, **6** (SeMe, SeAr): Y = H (**a**), OMe (**b**), and Cl (**c**)]. Non-bonded r(Se···Se) distances in **6a** (SeMe, SeAr), **6b** (SeMe, SeAr), and **6c** (SeMe, SeAr) are reported to be 3.070 Å [the average between 3.048(1) and 3.091(1) Å], 3.0951(8), and 3.1239(7) Å, respectively.[5e] The structures are **CC**, pseudo-**AB**, and pure-**AB**, respectively. The r(Se···Se) value becomes larger in an order of **CC** < pseudo-**AB** < pure-**AB**.

27 The structure of **III** was determined by means of X-ray crystallographic analysis: W. Nakanishi, S. Hayashi, unpublished results.

28 W. Nakanishi, S. Hayashi, D. Shimizu, M. Hada, *Chem.—Eur. J.* **2006**, *12*, 3829.

29 The values for **I** (**BB**) and **IV** (**AA**) are averaged values. And the observed values are from *p*-chlorophenyl group in place of phenyl groups.

30 A. Bondi, *J. Phys. Chem.* **1964**, *68*, 441.

31 J. C. Bryan, J. L. Lavis, R. A. Sachleben, *Acta Crystallogr., Sect. C* **1998**, *54*, 1662.

32 G. W. Buchanan, A. Rodrigue, K. Bourque, A. C. Chiverton, I. R. Castleden, S. Fortier, *Can. J. Chem.* **1994**, *72*, 1218.

33 M. Gerzain, G. W. Buchanan, A. B. Driega, G. A. Facey, G. Enright, R. A. Kirby, *J. Chem. Soc., Perkin Trans. 2* **1996**, 2687.

34 D. Sellmann, K. Engl, T. Gottschalk-Gaudig, F. W. Heinemann, *Eur. J. Inorg. Chem.* **1999**, 333.

35 N. Takeda, D. Shimizu, N. Tokitoh, *Inorg. Chem.* **2005**, *44*, 8561.

36 R. D. Calleja, E. S. Martínez, S. Friederichs, J. Kudnig, J. Bracker, G. Klar, *J. Mater. Chem.* **1995**, *5*, 389.

37 K. Akiba, M. Yamashita, Y. Yamamoto, S. Nagase, *J. Am. Chem. Soc.* **1999**, *121*, 10644.

38 M. Yamashita, Y. Yamamoto, K. Akiba, D. Hashizume, F. Iwasaki, N. Takagi, S. Nagase, *J. Am. Chem. Soc.* **2005**, *127*, 4354.

39 J. P. Fang, T. Lu, H. Kim, I. Delgado, P. Geoffroy, J. L. Atwood, G. W. Gokel, *J. Org. Chem.* **1991**, *56*, 7059.

40 S. M. Reed, T. J. R. Weakley, J. E. Hutchison, *Cryst. Eng.* **2000**, *3*, 85.

41 E. Espinosa, I. Alkorta, J. Elguero, E. Molins, *J. Chem. Phys.* **2002**, *117*, 5529.

42 W. Nakanishi, S. Hayashi, K. Narahara, *J. Phys. Chem. A* **2008**, *112*, 13593.